Nuclear Engineering and Technology 48 (2016) 72–86

Available online at ScienceDirect

Nuclear Engineering and Technology

journal homepage: www.elsevier.com/locate/net

Original Article

Ex-vessel Steam Explosion Analysis for Pressurized Water Reactor and Boiling Water Reactor

*Matjaž Leskovar** and *Mitja Uršič*

Jožef Stefan Institute, Jamova cesta 39, SI-1000 Ljubljana, Slovenia

ARTICLE INFO

Article history:
Received 8 June 2015
Received in revised form
20 August 2015
Accepted 23 August 2015
Available online 28 October 2015

Keywords:
Boiling Water Reactor
Fuel-Coolant Interaction
Pressure Load
Pressurized Water Reactor
Reactor Cavity
Severe Accident
Steam Explosion

ABSTRACT

A steam explosion may occur during a severe accident, when the molten core comes into contact with water. The pressurized water reactor and boiling water reactor ex-vessel steam explosion study, which was carried out with the multicomponent three-dimensional Eulerian fuel–coolant interaction code under the conditions of the Organisation for Economic Co-operation and Development (OECD) Steam Explosion Resolution for Nuclear Applications project reactor exercise, is presented and discussed. In reactor calculations, the largest uncertainties in the prediction of the steam explosion strength are expected to be caused by the large uncertainties related to the jet breakup. To obtain some insight into these uncertainties, premixing simulations were performed with both available jet breakup models, i.e., the global and the local models. The simulations revealed that weaker explosions are predicted by the local model, compared to the global model, due to the predicted smaller melt droplet size, resulting in increased melt solidification and increased void buildup, both reducing the explosion strength. Despite the lower active melt mass predicted for the pressurized water reactor case, pressure loads at the cavity walls are typically higher than that for the boiling water reactor case. This is because of the significantly larger boiling water reactor cavity, where the explosion pressure wave originating from the premixture in the center of the cavity has already been significantly weakened on reaching the distant cavity wall.

1. Introduction

Steam explosion, in the frame of nuclear reactor safety, is a process resulting from the interaction between the core melt (corium) and water [1,2]. Energy transfer from the corium to the coolant is so fast that a large amount of vapor is produced within a very short time. High pressure and fast expansion of vapor could potentially induce high loading on the surrounding structures. A steam explosion is also called an energetic fuel–coolant interaction (FCI). In the case of an ex-vessel steam explosion, cavity walls might not be able to bear such dynamic loads. Then, the cavity or even the

* *Corresponding author.*
E-mail address: matjaz.leskovar@ijs.si (M. Leskovar).

http://dx.doi.org/10.1016/j.net.2015.08.012
1738-5733/Copyright © 2015, Published by Elsevier Korea LLC on behalf of Korean Nuclear Society.

containment might be at risk of damage or even failure [3–5]. Direct or bypassed loss of the containment integrity can lead to the release of radioactive materials into the environment, threatening the safety of the general public.

Details of processes taking place prior to and during a steam explosion have been experimentally studied for a number of years, with adjunct efforts in modeling these processes to address the scaling of experimental results to reactor conditions [1,6,7]. Despite great efforts in steam explosion research, the confidence in predicting reactor situations is not such that an unambiguous decision can be taken whether there would be an early failure of the containment due to a steam explosion or not. To resolve the remaining open issues on the FCI processes and their effect on ex-vessel steam explosion energetics, the OECD project Steam Explosion Resolution for Nuclear Applications (SERENA) was launched in 2007, consisting of an experimental and an analytical part [8,9]. To verify the progress made in the understanding and modeling of key FCI processes for reactor applications, a reactor exercise was performed at the end of the project. The exercise comprises three cases: a pressurized water reactor (PWR) central melt release, a PWR side release, and a boiling water reactor (BWR) central release.

In our ex-vessel steam explosion study, conditions of the SERENA project reactor exercise for the PWR and BWR central melt release cases were considered. Simulations were carried out by applying two different jet breakup modeling approaches. In the following sections, the modeling approach and the considered ex-vessel FCI cases are described first. Next, the PWR and BWR simulations that were performed are presented. Various premixing and explosion-phase simulation results are provided and discussed. Finally, the PWR and BWR simulation results are discussed in comparison.

2. Modeling and calculation conditions

Simulations were performed with the computer code MC3D (multicomponent three-dimensional Eulerian fuel–coolant interaction code), version 3.6.8 [10,11]. MC3D is a multidimensional Eulerian code devoted to the study of multiphase and multiconstituent flows in the field of nuclear safety. The steam explosion simulation is usually carried out in two steps. First, the premixing phase is simulated followed by the simulation of the succeeding explosion phase, using the premixing simulation results as initial conditions and applying an explosion trigger.

In reactor calculations, the largest uncertainties in the prediction of the steam explosion strength are expected to be caused by the large uncertainties related to jet breakup. These uncertainties propagate through different premixing processes and result in uncertainties in the generation rate and size of the melt droplets, distribution of the melt droplets in the premixture, droplet solidification, and void fraction, all of which influence the steam explosion strength [9]. In MC3D, two jet breakup models are provided: a global model and a local one. The global jet breakup model is based on the hypothesis that jet breakup can be achieved through a correlation considering only the local physical properties of the melt, liquid, and vapor, without considering the local velocities. The local jet breakup model is based on the Kelvin–Helmholtz instability model, which also considers the local velocities. To get some insight into these uncertainties related to jet breakup, the premixing simulations were performed with both available jet breakup models.

The global jet breakup model is, strictly speaking, applicable only for single large, very hot jets in a water pool, so that fragmentation occurs due to the friction of the vapor film, whose characteristics are governed mainly by buoyant forces. The model was validated on the FARO facility steam explosion tests [12], so extrapolations to situations far from those of FARO are questionable. In this model, the rate of volumetric jet fragmentation into droplets is deduced from the comparison with a standard case:

$$\Gamma_f = \Gamma_0 \left(\frac{T_0}{T_j}\right)^{0.75} \sqrt{\frac{\mu_g}{\mu_{g,0}}\Big|_{p=1\text{bar}} \frac{\sigma_0}{\sigma_j}\left(\frac{\rho_0}{\rho_j}\right)^{0.5}}, \tag{1}$$

where typical FARO conditions are chosen for the standard case: reference fragmentation rate $\Gamma_0 = 0.1\ \text{m}^3/\text{m}^2/\text{s}$, jet temperature $T_0 = 3{,}000$ K, vapor viscosity $\mu_{g,0} = 10^{-3}$ kg/m/s, jet density $\rho_0 = 8{,}000\ \text{kg/m}^3$, and jet surface tension $\sigma_0 = 0.5$ N m. The diameter of the created droplets is a user input parameter with a default value of 3 mm, which is the typical average Sauter diameter in the FARO experiments.

The local jet breakup model is based on the Kelvin–Helmholtz instability model, which was modified to take into account the multiphase aspect. In this model, the volumetric jet fragmentation rate is calculated with the following equation:

$$\Gamma_f = N_f \frac{\sqrt{\rho_j \rho_{amb}\left(v_j - v_{amb}\right)^2 - \sigma_j k_{\max}\left(\rho_j + \rho_{amb}\right)}}{\rho_j + \rho_{amb}},$$
$$k_{\max} = \frac{2}{3}\frac{\rho_j \rho_{amb}}{\rho_j + \rho_{amb}}\frac{\left(v_j - v_{amb}\right)^2}{\sigma_j}, \tag{2}$$

where the subscript j stands for the jet and the subscript amb stands for the ambient fluid, the properties of which are calculated by averaging considering the phases volume fractions. N_f is the jet fragmentation parameter with an expected value between 1 and 6. Direct comparisons with the FARO experiments lead to the use of $N_f = 2$ [13]. In this model, the diameter of the created droplets d_d is related to the wavelength λ of instability, which is established from the wave number $k_{\max}$ [Eq. (2)]:

$$d_d = N_d \lambda \ , \quad \lambda = \frac{2\pi}{k_{\max}} \ . \tag{3}$$

N_d is the droplet diameter parameter with an expected value between 0.1 and 0.5; the recommend value, based on comparisons with the FARO experiments, is $N_d = 0.2$ [13].

In this study, conditions of the SERENA project reactor exercise for the PWR and BWR central melt release cases were considered. A purpose of the reactor exercise was to verify whether the pressure loads calculated by various FCI codes are consistent with each other. This objective can be reached by applying the codes to a limited number of geometries and conditions that are generic enough to hold all the

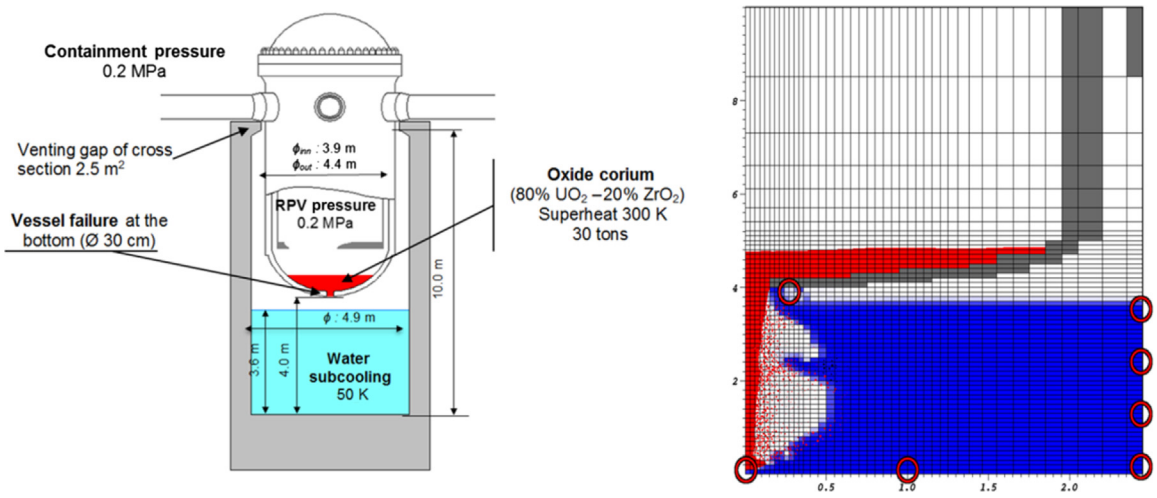

Fig. 1 – PWR scheme with initial conditions [14] and calculation model (vertical/horizontal scale = 0.3). The circles denote the locations where pressure loads were recorded. PWR, pressurized water reactor; RPV, reactor pressure vessel.

characteristics of reactor-scale FCI processes, and also realistic, meaning that they should correspond to plausible accident scenarios. In the SERENA project, representatives of the utilities provided the conditions that they consider most relevant according to their main reactor designs, e.g., the Electricity of France for their PWR and the Technical Research Centre of Finland for their BWR, based on which the three general reactor exercise cases were defined: PWR central release, PWR side release, and BWR central release [14]. As revealed in the OECD MASCA project experiments, the melt pool in the lower head may gradually stratify into three layers of different melt compositions—a molten oxidic pool with a

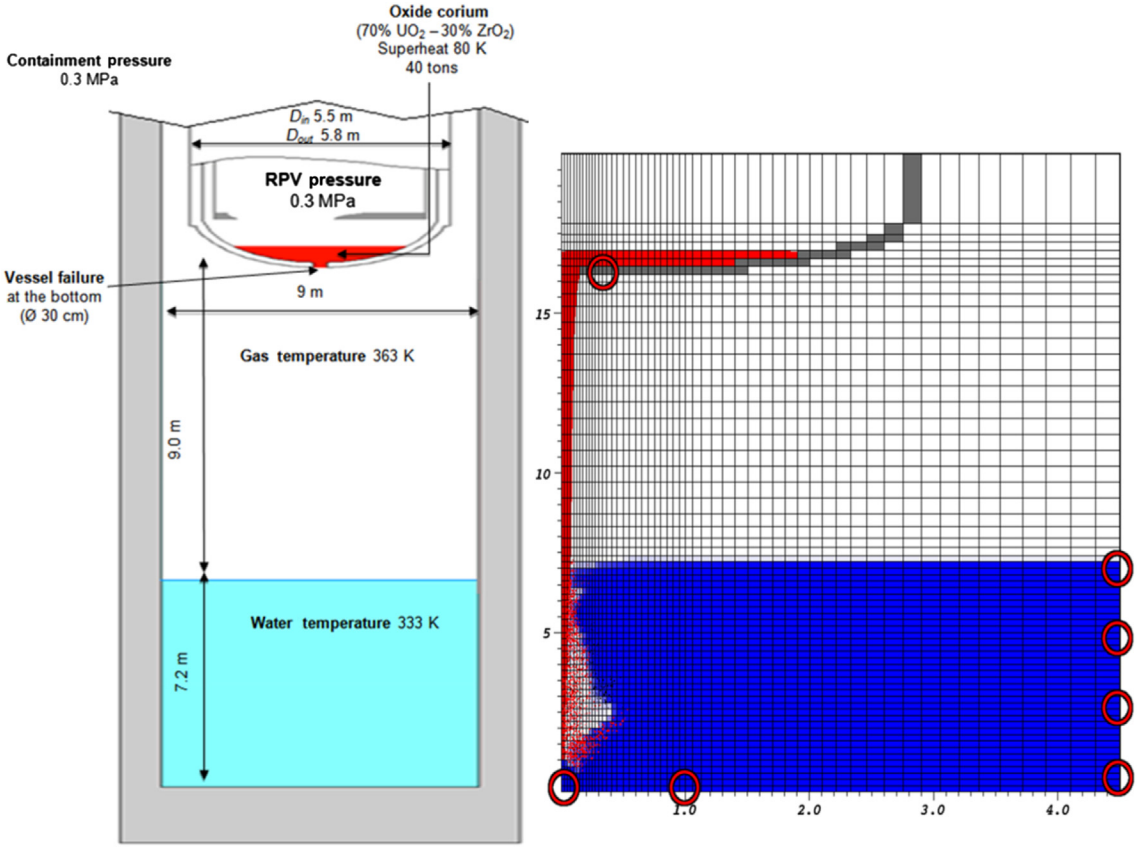

Fig. 2 – BWR scheme with initial conditions [14] and calculation model (vertical/horizontal scale = 0.3). The circles denote the locations where pressure loads were recorded. BWR, boiling water reactor; RPV, reactor pressure vessel.

Table 1 – Main initial conditions for PWR and BWR cases.

	PWR	BWR
Melt temperature (K)	3,228	2,950
Melt superheat (K)	300	80
Melt mass (t)	30	40
Melt pour	By gravity	By gravity
Jet discharge diameter (m)	0.3	0.3
Free fall height (m)	0.4	9
Water height (m)	3.6	7.2
Water temperature (K)	343	333
Water subcooling (K)	50	74
Pressure (MPa)—vessel/containment	0.2/0.2	0.3/0.3

BWR, boiling water reactor; PWR, pressurized water reactor.

light metal layer on top and a heavy metal layer below [15]. The light metal layer on top may focus the heat on a narrow reactor vessel region, so a vessel failure on the side, resulting in a side melt release, is more probable than a vessel failure at the bottom, resulting in a central release. Simulation of a side melt release has large uncertainties due to the required three-dimensional modeling approach and the lack of experimental validation possibilities. Thus, in the present study, only the central release cases were considered. It should be stressed that neither the SERENA reactor exercise nor our performed study are safety analyses. For a safety analysis, reactor-specific geometry and the wide spectrum of relevant severe accident scenarios would have to be considered. However, the performed study provides an interesting insight into the ex-vessel steam explosion behavior and the resulting pressure loads.

Geometries of the considered PWR and BWR cases with initial conditions are presented in Figs. 1 and 2. The molten corium is poured from the failed reactor vessel through an opening with a diameter of 30 cm into the cavity, which is partly filled with subcooled water. The containment and vessel pressures being equal, the melt is released solely by gravity. The main differences between the cases are that the cavity, free fall height, and water depth in the BWR case are significantly larger than those in the PWR case. The main initial conditions are summarized in Table 1. The geometry of the considered PWR and BWR cases is axial symmetric, thus enabling a two-dimensional modeling approach in the cylindrical coordinate system (Figs. 1 and 2). The mesh was adequately refined in the most important regions, i.e., in the area around the jet and in the water where the FCI occurs. After some testing, for the PWR case, a mesh of 42 (radial) × 59 (vertical) cells and for the BWR case, a mesh of 55 × 65 cells were chosen. At the upper boundary of the simulation domain, a constant-pressure boundary condition was applied. Compositions and properties of the corium used, which were provided in the SERENA project by the French Atomic Energy and Alternative Energies Commission for the PWR case and by Technical Research Centre of Finland for the BWR case [14], are given in Table 2. The thermodynamic properties of corium were calculated with the GEMINI2 code [16] using the NUCLEA-09 thermodynamic database [17].

3. Simulation of PWR case

3.1. *Premixing phase*

The premixing phase was simulated 2.5 seconds after the start of the melt release. Two simulations were performed: one applying the global jet breakup model (named the global model) and the other applying the local jet breakup model (named the Kelvin–Helmholtz model or KH model). Default or recommended modeling parameters were used.

In Fig. 3, the premixing conditions calculated with the global and KH models are presented for various times after the melt release. After a free fall of 0.4 m through the gas, the corium jet starts to penetrate the water and gradually breaks up into melt droplets. The red dots denote the regions with the melt droplets that are hot enough to be considered as effectively liquid, and the black dots denote the regions with droplets that are considered to be effectively solid and thus are not able to undergo fragmentation. The melt droplets are considered to be effectively liquid if their average temperature is higher than the melt solidus temperature. This is the default criterion, which takes into account the fact that the MC3D code is based on the average Sauter diameter of the melt droplets. In the later stage of the simulations, after the melt–bottom contact, due to some violent interactions, fluid flow becomes very turbulent and the premixture is pushed inside the reactor vessel. With the global model, this is related to the secondary breakup, where strong coupling of the droplets size, heat transfer rate, and droplet fragmentation, which is promoted by the resulting rapid void buildup, may lead to an intensive interaction. With the KH model,

Table 2 – Applied corium material properties for PWR and BWR cases.

	PWR	BWR
Material	80 wt% UO_2/20 wt% ZrO_2	70 wt% UO_2/30 wt% ZrO_2
Density (kg/m^3)	7,300	8,000
Thermal conductivity (W/m/K)	3.00	2.88
Specific heat (J/kg/K)—solid/liquid	450/510	450/510
Latent heat (kJ/kg)	280	320
Temperature (K)—solidus/liquidus	2,882/2,928	2,840/2,870
Surface tension (N/m)	0.573	0.45
Emissivity	0.8	0.79
Dynamic viscosity (Pa·sec)	0.005	0.008

BWR, boiling water reactor; PWR, pressurized water reactor.

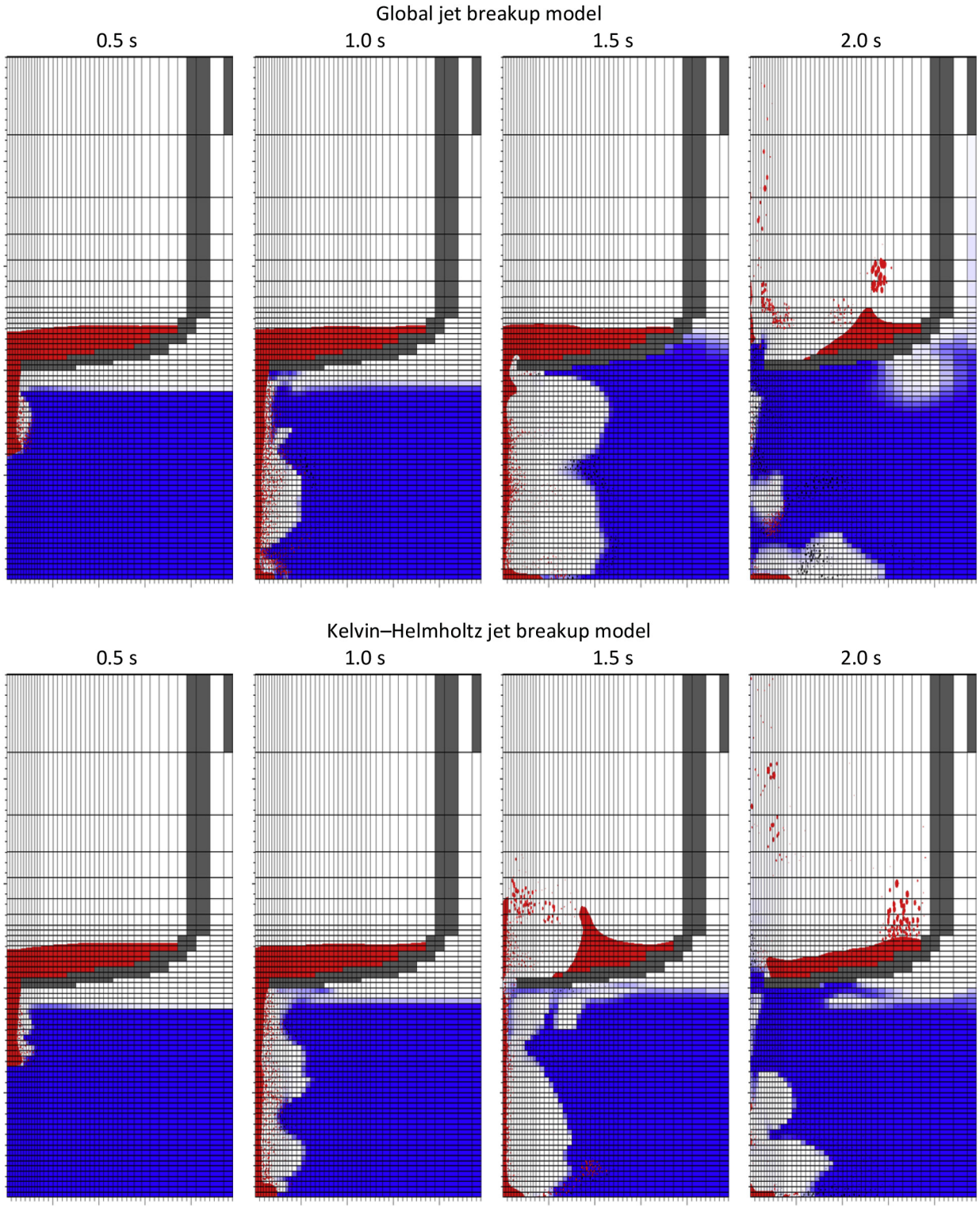

Fig. 3 – Premixing conditions at various times after melt release calculated using the global and Kelvin–Helmholtz jet breakup models (vertical/horizontal scale = 0.6).

this is related to the strong feedback mechanisms of the jet breakup itself, where the jet fragmentation rate and the size of the created droplets directly depend on the ambient pre-mixture conditions.

In Fig. 4, evolution of the overall melt droplets average Sauter diameter is presented. In the global model, the size of the created droplets is a user parameter and the default value of 3 mm was used. Thus, the average size of the droplets is

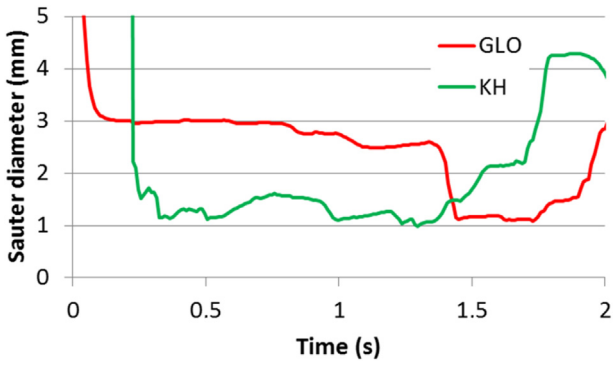

Fig. 4 – Melt droplets average Sauter diameter for simulations with the global and Kelvin–Helmholtz jet breakup models. GLO, global jet breakup model; KH, Kelvin–Helmholtz jet breakup model.

initially 3 mm (when no droplets are present, the Sauter diameter is arbitrarily set to a large value due to numerical reasons) and then reduced due to secondary breakup, resulting in fragmentation of unstable droplets into smaller droplets. At about 1.5 seconds, intensive fragmentation occurs, as explained in the previous paragraph, rapidly decreasing the droplet size to about 1 mm. In the KH model, the size of the melt droplets created depends on the local conditions, and it is in the range of 1–2 mm. At the end of the simulations, droplet size increases with both jet breakup models. The reason for this is that due to the turbulent fluid flow, the continuous melt phase becomes too distorted to be well described by the rough mesh and numerically breaks up into large droplets (Fig. 3).

Fig. 5 shows the evolution of various corium masses, which are as follows: total mass of corium in water, total mass of corium droplets, mass of liquid droplets, total mass of droplets in regions with less than 60% of void, and mass of liquid droplets in regions with less than 60% of void. The total mass of corium in water is defined as the mass of corium below the initial water level. Thus, when violent interactions occur and the premixture is also pushed inside the reactor vessel (Fig. 3), various droplet masses may become larger than the so defined mass of corium in water.

The strength of a steam explosion depends on the mass of melt droplets that can efficiently participate in the steam explosion—that is, the mass of liquid melt droplets in regions with high water content, the so-called active melt mass. The mass of liquid droplets in regions with less than 60% of void is a good measure for this active melt mass (Fig. 5, curve "DrLiq& < 60%"). The total mass of droplets in regions with less than 60% of void shows the limiting effect on the explosion strength solely by void (curve "DrVap < 60%"), and the mass of liquid droplets shows the limiting effect solely by solidification (curve "DrLiquid").

In the initial melt penetration stage up to about 1 second, the mass of corium in water is similar in both cases (Fig. 5, curve "InWater"). This was expected because due to the applied constant-pressure boundary condition, pressure buildup below the vessel is negligible, resulting in an unrestricted gravity pour of the melt. Once the water level reaches the reactor vessel (Fig. 3), pressure starts to build up in the central part of the cavity and thus reducing melt outflow. When a violent interaction occurs, the pressure buildup is so large that no melt can flow out of the vessel anymore. Actually, the premixture is pushed inside the vessel. This happens somewhat earlier with the KH model, so the final mass of corium in water is lower than that for the global model. As the system shows a complex behavior after the violent interaction, we will focus our discussion only on the initial melt penetration stage up to the melt–bottom contact (Fig. 5, dotted black line). It may be observed that the total mass of droplets is greater with the global model (curve "Droplets"). As expected, melt solidification is much more expressed with the KH model due to smaller droplets, which cool faster (compare curves "Droplets" and "DrLiquid"). However, the ratio of the mass of droplets in high-

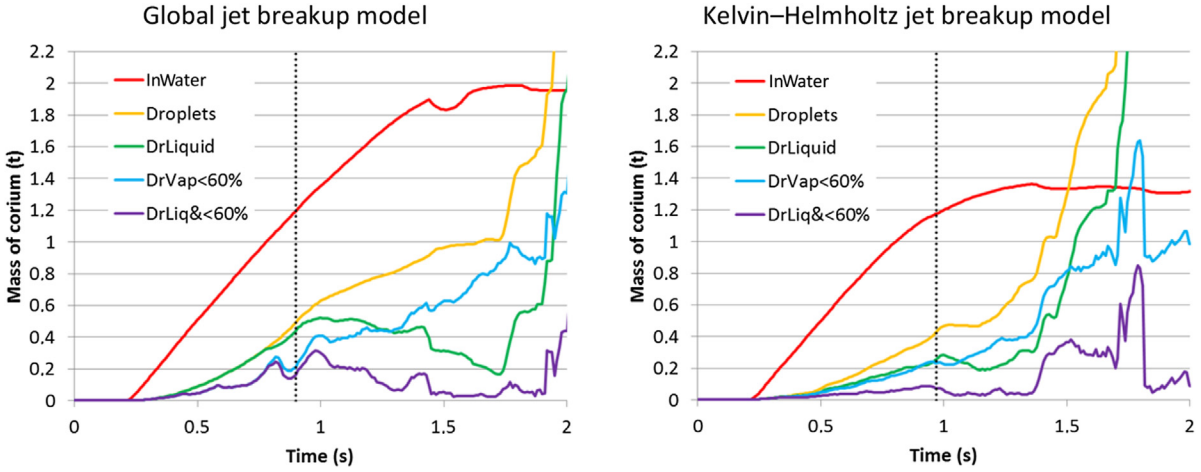

Fig. 5 – Evolution of various corium masses (InWater, Droplets, DrLiquid, DrVap < 60%, and DrLiq& < 60%) for simulations with the global and Kelvin–Helmholtz jet breakup models. The dotted black line denotes the time of the melt–bottom contact (i.e., the explosion triggering time). DrLiquid, mass of liquid droplets; DrLiq& < 60%, mass of liquid droplets in regions with less than 60% of void; Droplets, total mass of corium droplets; DrVap < 60%, total mass of droplets in regions with less than 60% of void; InWater, total mass of corium in water.

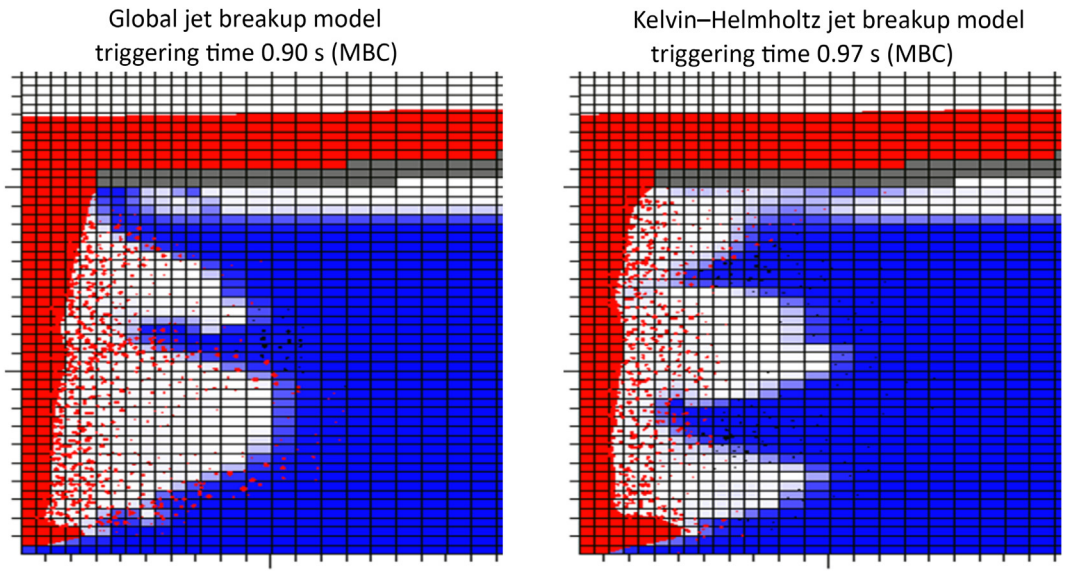

Fig. 6 – Premixture conditions at explosion triggering time for simulations with the global and Kelvin–Helmholtz models. MBC, melt–bottom contact time.

voided regions to the total mass of droplets is comparable for both models (compare curves "Droplets" and "DrVap < 60%"). A significant difference was expected because the smaller droplets of the KH model produce more void. However, the reason for this result is the jet breakup modeling itself. In the global model, the fragmentation rate does not depend on the local premixture conditions. Melt droplets are created even when the jet is surrounded by a thick vapor chimney, and so these droplets are inserted directly into the gas region (Fig. 3). The most important result is the active mass (curve "DrLiq& < 60%), i.e., the mass of liquid melt droplets in low-voided regions, because it can be related to the expected strength of the steam explosion. The active mass is typically lower with the KH model due to the smaller droplets; therefore, stronger explosions are expected with the global model. The triggering time is denoted by the black dotted line.

3.2. *Explosion phase*

For each premixing simulation, an explosion simulation was performed. The explosion phase was simulated 100 milliseconds after triggering. The explosion was triggered at the melt–bottom contact time by applying a triggering cell with pressurized gas at 5 MPa at the bottom of the cavity in the center. This triggering time was chosen because, in experiments, spontaneous steam explosions were often triggered when the melt reached the bottom [2].

In Fig. 6, premixture conditions at the explosion triggering time are presented for the simulations with the global and KH models. It may be observed that the region of liquid droplets (red dots) in water (blue region) is larger for the global model, which is in accordance with the active mass curves in Fig. 5.

In Fig. 7, the time evolution of the calculated pressures and the corresponding pressure impulses (integral of pressure over time) are presented for the locations marked in Fig. 1. These locations are as follows: cavity bottom at the center (curve "CavBotCen"), cavity bottom 1 m from the center (CavBot1m), cavity wall at elevations of 0.5–3.5 m (WalEle0.5m–WalEle3.5m), and reactor vessel 0.25 m from the center (VesCen0.25m). In all the cases, the largest pressures and pressure impulses are calculated on the cavity bottom in the center. Loads on the wall are lower because pressure is reduced during the propagation of the explosion pressure wave from the premixture region to the wall in the axial symmetric geometry and they also decrease with increased elevation due to the pressure relief. In accordance with the calculated active mass at triggering time (Fig. 5, curve "DrLiq& < 60%"), pressure loads are smaller with the KH model compared to those with the global model. One exception is the narrow pressure peak on the cavity bottom in the center, which is larger with the KH model (~53 MPa vs. ~39 MPa) and is a local event. It may be observed that the cavity wall is periodically loaded due to pressure reflections. The maximum pressure on the wall is ~15 MPa for both models, but the maximum pressure impulse on the wall is significantly lower with the KH model (~80 kPa·second vs. ~110 kPa·second). The pressure impulse on the bottom of the cavity in the center is ~140 kPa·second for both models. With the KH model, the pressure impulse decreases rapidly with increasing distance from the center. At a distance of 1 m from the center, the pressure impulse drops to ~80 kPa··second with the KH model, whereas it is still ~110 kPa··second with the global model.

4. Simulation of BWR case

4.1. *Premixing phase*

The premixing phase was simulated 2.5 seconds after the start of the melt release. Similar to the PWR case, two simulations were performed, one applying the global model and the other

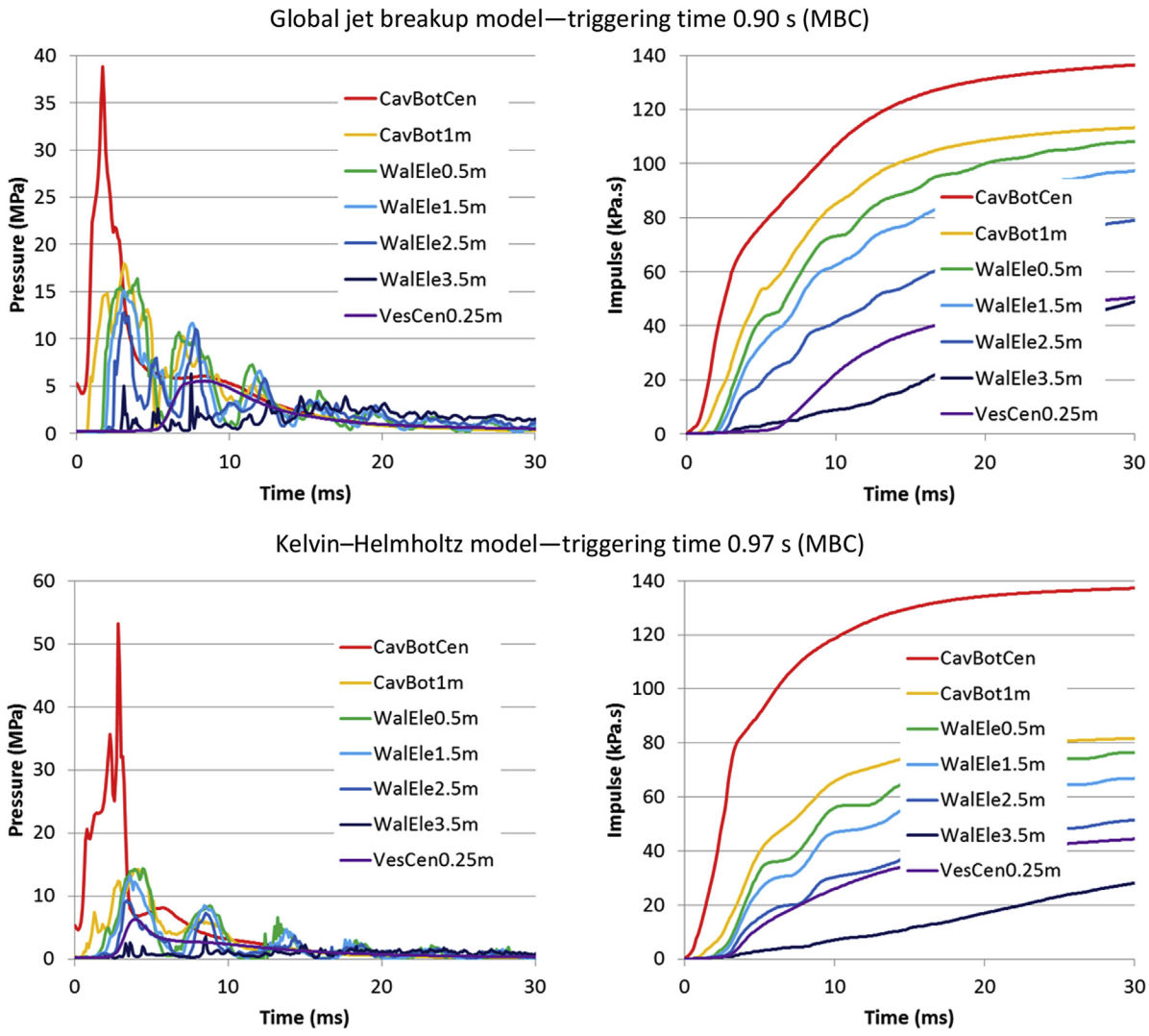

Fig. 7 – Pressure at locations marked in Fig. 1 with corresponding pressure impulses, applying the global and Kelvin–Helmholtz jet breakup models in the premixing calculation. CavBotCen, cavity bottom at the center; CavBot1m, cavity bottom 1 m from the center; VesCen0.25m, reactor vessel 0.25 m from the center; WalEle0.5m, cavity wall at an elevation of 0.5 m; WalEle1.5m, cavity wall at an elevation of 1.5 m; WalEle2.5m, cavity wall at an elevation of 2.5 m; WalEle3.5m, cavity wall at an elevation of 3.5 m.

applying the local KH model. Calculation with the global model became unstable after 2.28 seconds and stopped; thus, only those results that were obtained till the calculation stopped are presented.

In Fig. 8, the premixing conditions at various times after the melt release are presented for both calculations performed. The same denotation as in Fig. 3 is used here. After a free fall of 9 m through the gas, the corium jet starts to penetrate the water and gradually breaks up into melt droplets. With the global model, the jet breakup is insignificant until the melt penetrates the water, whereas with the KH model, the jet breakup becomes significant during the free fall through the gas.

In Fig. 9, evolution of the melt droplets average Sauter diameter is presented. In the global model, the default size of 3 mm was used for the droplets created. Thus, the average size of the droplets is initially 3 mm. At about 2 seconds, intensive fragmentation occurs, as was also observed in the PWR case, rapidly decreasing the droplet size to about 1 mm. This violent interaction is caused by the strong coupling of the droplets size, heat transfer rate, and resulting rapid void buildup, which promotes droplet fragmentation. In the KH model, the size of the created melt droplets is calculated and it is in the range of 1–2 mm. Due to the smaller droplet size and thus larger heat transfer area, the void buildup with the KH model is larger than that with the global model (Fig. 8).

In Fig. 10, evolution of various corium masses in water is presented. Here, the same corium masses as in Fig. 5 for the PWR case are shown, where the figure description is also provided. The jet breakup modeling has no significant influence on the melt release; thus, the mass of corium in water is similar in both cases (Fig. 10, curve "InWater"). In the initial

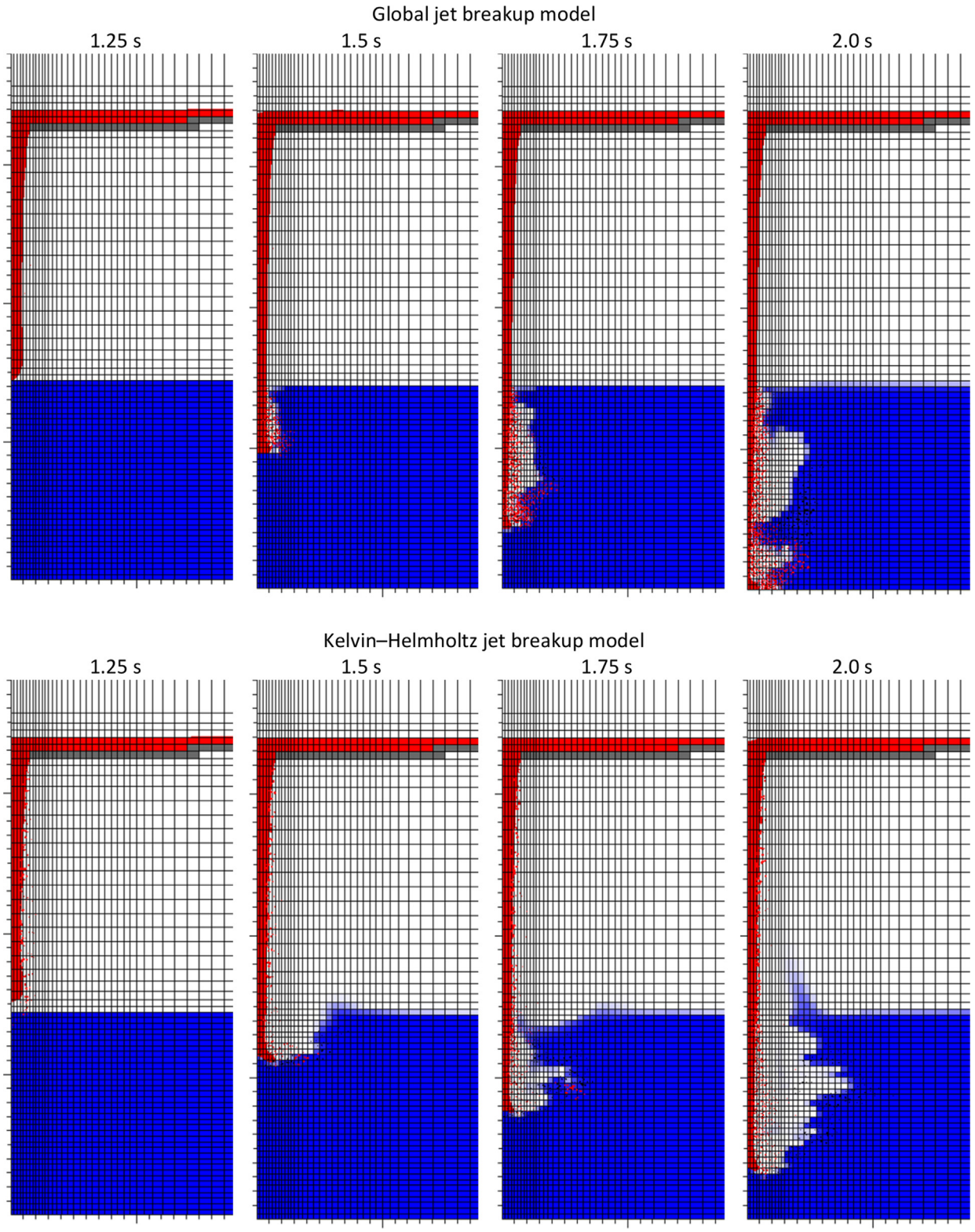

Fig. 8 – Premixing conditions at various times after the melt release calculated using the global and Kelvin–Helmholtz jet breakup models (vertical/horizontal scale = 0.2).

melt penetration stage up to about 2 seconds, the total mass of melt droplets is typically larger with the global model; later, it is larger with the KH model (curve "Droplets"). It seems that the fragmentation rate per jet length is typically larger with the KH model, and that the differences in the initial stage occur due to a faster jet penetration with the global model and thus initially a longer jet length in the water. As expected, melt solidification is much more expressed with the KH model due

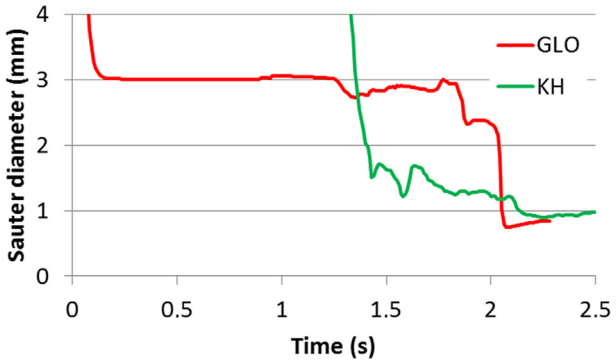

Fig. 9 – Melt droplets average Sauter diameter for simulations with the global and Kelvin–Helmholtz models. GLO, global jet breakup model; KH, Kelvin–Helmholtz jet breakup model.

to the smaller droplets, which cool faster (curve "DrLiquid"). Surprisingly, the mass of droplets in high-voided regions is higher with the global model (compare curves "Droplets" and "DrVap < 60%"). The opposite was expected since the smaller droplets with the KH model produce more void. Similar to in the PWR case, the reason for this behavior is the jet breakup modeling itself. In the global model, the fragmentation rate under the water level does not depend on the local conditions. Melt droplets are also created if the jet is surrounded by a thick vapor chimney and thus these droplets are inserted directly into the gas region (Fig. 8). The most important result is the active mass (curve "DrLiq& < 60%"), i.e., the mass of liquid melt droplets in low-voided regions, because it defines the expected strength of the steam explosion. The active mass is typically lower with the KH model due to the smaller droplets (before the discussed intensive fragmentation occurs with the global model after 2 seconds), so stronger explosions are expected with the global model.

4.2. *Explosion phase*

The explosion phase was simulated 100 milliseconds after triggering. The explosion was triggered by applying a triggering cell with pressurized gas at 5 MPa. For each premixing simulation two explosion simulations were performed:

- Case "Front 3.6 m": The explosion was triggered when the melt penetrated 3.6 m into the water, as in the PWR case, in order to make direct comparisons. The triggering cell was just below the melt front on the symmetry axis. The triggering time was 1.62 seconds for the premixing calculation with the global model and 1.75 seconds with the KH model.
- Case "Maximum active mass": As it was presumed that the melt might already be solidified when it reaches the bottom of the deep BWR water pool, thus not enabling self-triggering at that location, the explosion was not triggered at the melt–bottom contact time, like in the PWR case, but at the time of the maximum calculated active mass (Fig. 10, curve "DrLiq& < 60%") when the strongest explosion is expected. The triggering cell was at the cavity bottom on the symmetry axis. As the explosion calculation with the global model did not converge for these conditions, the triggering cell was lifted by one cell that should have no important influence on the results. The triggering time was 1.88 seconds for the premixing calculations with the global model and 1.67 seconds with the KH model.

The premixture conditions at the explosion triggering times for the considered cases are presented in Fig. 11. It may be observed that the region of liquid droplets (red dots)

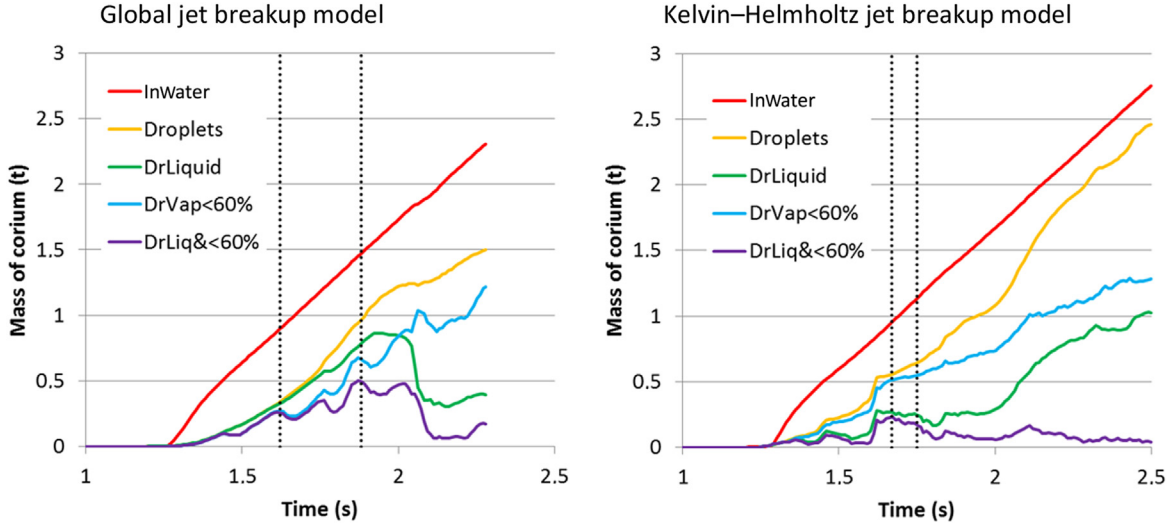

Fig. 10 – Evolution of various corium masses (InWater, Droplets, DrLiquid, DrVap < 60%, and DrLiq& < 60%) for simulations with the global and Kelvin–Helmholtz jet breakup models. The dotted black lines denote the times when the explosion was triggered. DrLiquid, mass of liquid droplets; DrLiq& < 60%, mass of liquid droplets in regions with less than 60% of void; Droplets, total mass of corium droplets; DrVap < 60%, total mass of droplets in regions with less than 60% of void; InWater, total mass of corium in water.

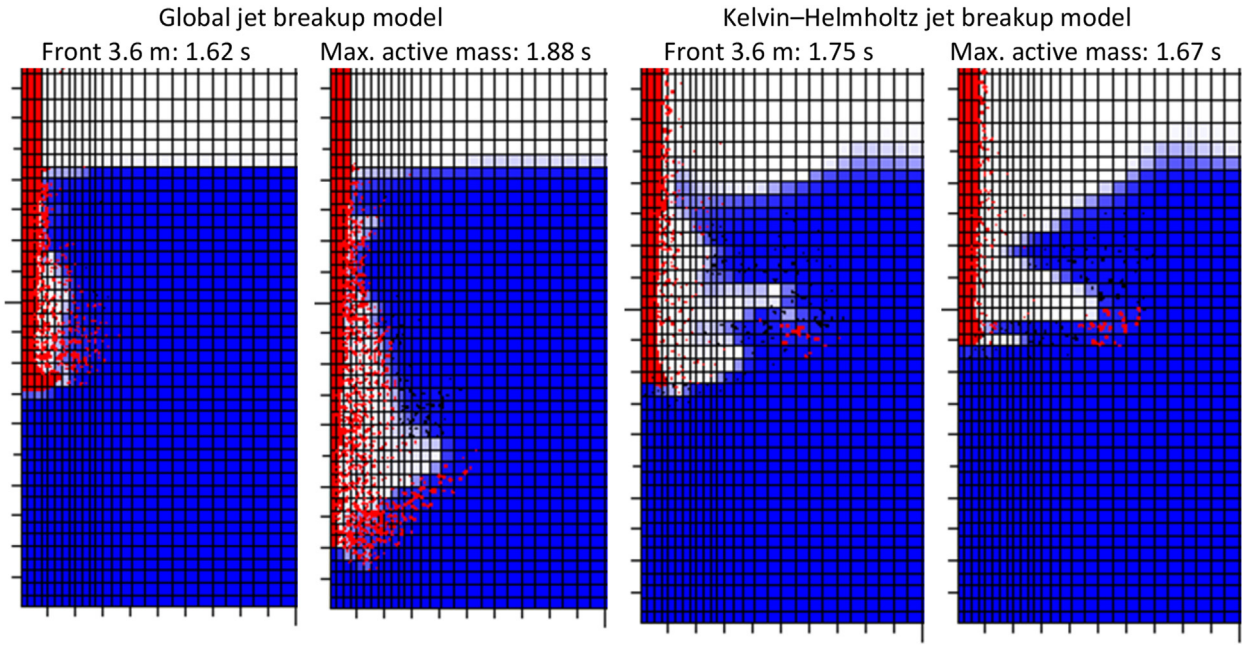

Fig. 11 – Premixture conditions at explosion triggering time for simulations with the global and Kelvin–Helmholtz models for both triggering cases (vertical/horizontal scale = 0.2).

in liquid water (blue region) is larger for the global model, which is in accordance with the active mass curves in Fig. 10.

In Figs. 12 and 13, the time evolution of the calculated pressures and the corresponding pressure impulses are presented for the locations marked in Fig. 2. These locations are as follows: cavity bottom at the center (curves "CavBotCen"), cavity bottom 1 m from the center (CavBot1m), wall at elevations of 1–7 m (WalEle1m–WalEle7m), and reactor vessel 0.25 m from the center (VesCen0.25m). In all cases, the maximum pressures and pressure impulses are calculated at the cavity bottom in the center. The loads on the wall are lower, since the pressure is reduced during propagation of the explosion pressure wave from the pressure region to the wall in the axial symmetric geometry, and they also decrease with increased elevation due to pressure relief. The maximum pressures at the cavity bottom are comparable for all considered cases (~25 MPa). Pressure peaks with the KH model are very narrow, less than 1 millisecond. The maximum pressures at the wall are significantly higher with the global model (about 15–20 MPa) than with the KH model (about 5–10 MPa), but the duration of the elevated pressure is similar (~7 milliseconds). As expected based on the active mass curves (Fig. 10, curves "DrLiq& < 60%"), pressure impulses are significantly higher with the global model than with the KH model. With the global model, the maximum pressure impulse at the wall is ~60 kPa·second for the triggering case "Front 3.6 m" and ~90 kPa·second for the case "Maximum active mass". With the KH model, the maximum pressure impulse at the wall is ~35 kPa·second for both triggering cases, which were triggered nearly at the same time (only 0.08-second difference).

5. Discussion

The discussion in this section focuses mainly on the comparative analysis of the PWR and BWR melt release cases considered, which were extensively discussed in the third and fourth sections, respectively. In Table 3, the main integral results of the simulations performed are presented for comparison. The typical melt mass outflow rate is larger for the BWR case than for the PWR case due to the higher melt pool in the reactor vessel and consequently a larger hydrostatic pressure at the vessel opening in the BWR case, resulting in a larger melt outflow velocity. The time from the start of the melt release till the melt–water contact is significantly larger for the BWR case due to the larger free fall height. Due to the higher melt–water impact velocity in the BWR case, the melt penetrates 3.6 m into the water when the explosion is triggered, significantly faster in the BWR case than in the PWR case. Thus, the mass of corium in water at this triggering time is lower for the BWR case despite the larger melt mass outflow rate. Due to the faster melt penetration and shorter melt penetration time till the triggering of explosion in the BWR case, resulting in less melt solidification and less void buildup, which is further reduced due to higher water subcooling, the active melt mass at the triggering of explosion is significantly larger for the BWR case. With the KH model the size of the created melt droplets is calculated and with a larger melt water penetration velocity the size of the created droplets is smaller. Consequently, one would expect a smaller average melt droplet size for the BWR case where the melt–water impact velocity is significantly larger than for the PWR case due to the large free fall height. However, it was found that the melt jet starts to break up during the long free fall through gas, where due to a low gas density larger melt droplets are

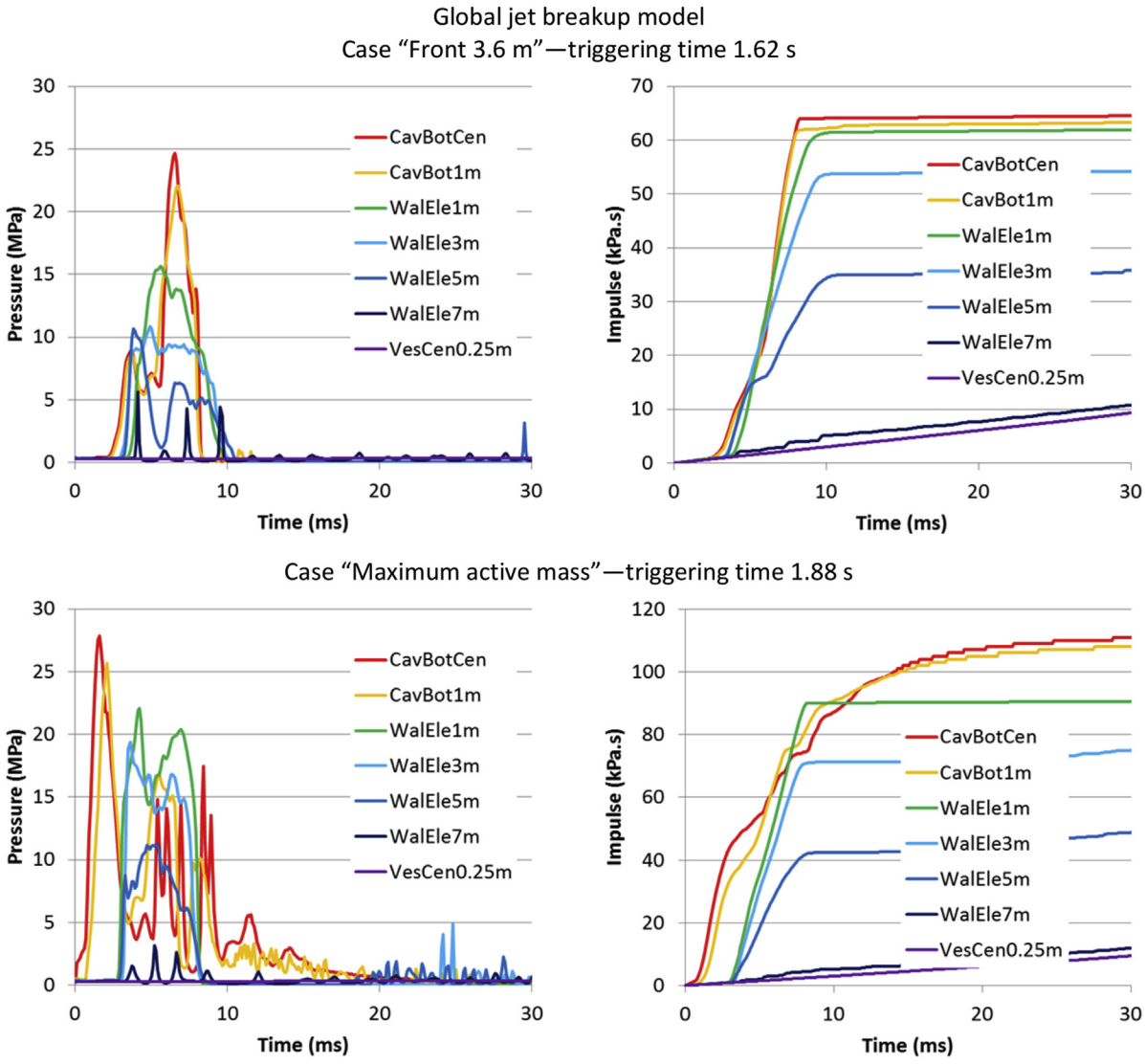

Fig. 12 – Pressures with corresponding pressure impulses at locations marked in Fig. 2 for both triggering cases, applying the global jet breakup model in the premixing calculation. CavBotCen, cavity bottom at the center; CavBot1m, cavity bottom 1 m from the center; VesCen0.25m, reactor vessel 0.25 m from the center; WalEle1m, wall at an elevation of 1 m; WalEle3m, wall at an elevation of 3 m; WalEle5m, wall at an elevation of 5 m; WalEle7m, wall at an elevation of 7 m.

created. Thus, with the KH model, the average Sauter diameter at the triggering time is even larger for the BWR case in comparison to that for the PWR case.

Despite the lower active melt mass for the PWR case, pressure loads at the cavity walls are higher than for the BWR case, where the explosion was triggered when the melt penetrated 3.6 m into the water. Pressure loads are typically even higher than those for the BWR case when the explosion is triggered at the time of the maximum active melt mass. Only the maximum pressure at the cavity wall is higher for the BWR case, applying the global model, than for the corresponding PWR case. Pressure loads in the BWR case are typically lower than those in the PWR case due to the significantly larger size of the BWR cavity. Specifically, the premixture in the center of the cavity, where the explosion occurs, is much more distant from the cavity wall than in the smaller PWR cavity, and thus when the pressure wave in the cylindrical cavity geometry reaches the BWR cavity wall it has already been weakened significantly.

During the steam explosion, thermal energy of the corium is converted into mechanical work. An important measure of the strength of the steam explosion is the mechanical work performed by the steam explosion, which initially reflects in the form of the kinetic energy of the corium, water, and vapor, being accelerated by the high pressure of the steam explosion. In Table 3, the calculated maximum total kinetic energy of these phases during the steam explosion is provided. As expected, the maximum kinetic energy is largest for the case with the largest active melt mass at triggering, i.e., the BWR case, applying the global jet breakup model, which was triggered at the time of the maximum active melt mass. It may be observed that at similar active melt masses, the maximum

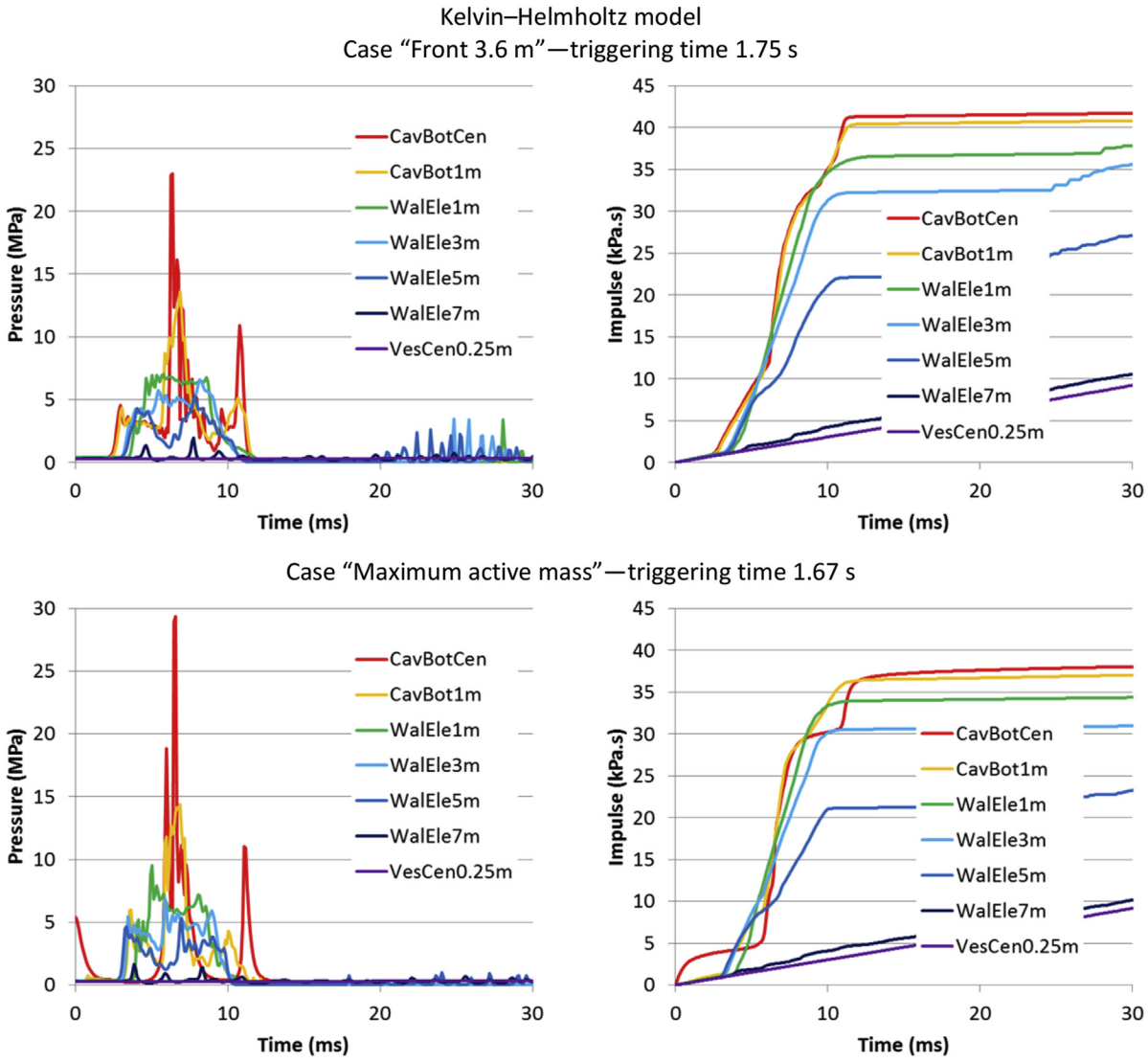

Fig. 13 – Pressures with corresponding pressure impulses at locations marked in Fig. 2 for both triggering cases, applying the Kelvin–Helmholtz jet breakup model in the premixing calculation. CavBotCen, cavity bottom at the center; CavBot1m, cavity bottom 1 m from the center; VesCen0.25m, reactor vessel 0.25 m from the center; WalEle1m, wall at an elevation of 1 m; WalEle3m, wall at an elevation of 3 m; WalEle5m, wall at an elevation of 5 m; WalEle7m, wall at an elevation of 7 m.

kinetic energy is significantly larger for the PWR case than for the BWR case (34.8 MJ with 193 kg active melt vs. 19.9 MJ with 168 kg active melt). The reason for this more efficient energy transfer from the active melt in the PWR case is that in the PWR case, the water level rises up to the reactor vessel (Fig. 6), making venting of the explosion region more difficult, whereas in the BWR case, the water surface is free (Fig. 11). Due to the longer confinement time of the explosion region, heat transfer from the active melt to the water is more completed in the PWR case.

The energy conversion ratio, which is defined as the ratio of the kinetic energy of the phases after the explosion to the initial thermal energy of the melt, is a convenient dimensionless integral steam explosion quantity for the characterization of steam explosion, enabling a basic quantitative comparison of various steam explosion experiments and analyses. In steam explosion experiments, the energy conversion ratio is usually calculated based on the total mass of melt in water at the triggering time. Often, the experiments are so designed that at the triggering time, the melt is mainly in the form of droplets. The energy conversion ratio was, therefore, calculated based on the total mass of corium in water and the mass of corium droplets in water (Table 3). The specific initial thermal energy of the melt, which is defined as the energy released when the melt cools from the initial melt temperature to the water temperature, is 1.58 MJ/kg for the PWR case and 1.49 MJ/kg for the BWR case (calculated from data of Tables 1 and 2). The results show that the energy conversion ratio is, in general, largest for the BWR case, applying the global jet breakup model (up to 3%, based on the total mass of corium in water). The reason is that, in the BWR case, due to faster melt penetration than in

Table 3 – Main integral results of PWR and BWR simulations performed, applying the global and Kelvin–Helmholtz jet breakup models.

Case	PWR		BWR			
Typical melt mass outflow rate (kg/sec)	~1,800		~2,200			
Melt–water impact velocity (m/sec)	4.2		11.5			
Melt–water contact time (sec)	0.21		1.26			
Jet breakup model	GLO	KH	GLO		KH	
Trigger selection	MBC	MBC	3.6 m	MAM	3.6 m	MAM
Trigger time (sec)	0.90	0.97	1.62	1.88	1.75	1.67
Melt penetration time at trigger (sec)	0.69	0.76	0.36	0.62	0.49	0.41
Mass of corium in water at trigger (kg)	1,209	1,180	896	1,472	1,140	958
Mass of corium droplets at trigger (kg)	509	443	336	960	647	558
Active mass of corium at trigger (kg)	193	71	259	494	168	230
Average Sauter diameter at trigger (mm)	2.78	1.15	2.88	2.32	1.37	1.64
Maximum pressure at cavity bottom (MPa)	38.8	53.2	22.5	27.8	23.0	29.4
Maximum pressure impulse at bottom (kPa·sec)	137	137	65	111	42	38
Maximum pressure at cavity wall (MPa)	16.4	14.2	15.7	22.1	7.0	9.5
Maximum pressure impulse at wall (kPa·sec)	108	76	62	91	38	34
Maximum kinetic energy of all phases (MJ)	34.8	19.4	35.2	65.3	19.9	13.8
Energy conversion ratio (%) based on:						
Mass of corium in water	1.8	1.0	2.6	3.0	1.2	1.0
Mass of corium droplets in water	4.3	2.8	7.0	4.6	2.1	1.7

For the PWR case, the explosion was triggered at the melt–bottom contact time and for the BWR case, it was triggered when the melt penetrated 3.6 m into the water and at the time of the maximum active mass.
BWR, boiling water reactor; GLO, global jet breakup model; KH, Kelvin–Helmholtz jet breakup model; MAM, maximum active mass; MBC, melt–bottom contact time; PWR, pressurized water reactor.

the PWR case and larger melt droplets than with the KH jet breakup model, a premixture with less void and less melt solidification forms compared to that in other cases, leading to the most efficient explosion. This is also reflected in the largest active mass of corium with regard to the total mass of corium in water for the BWR case, with global jet breakup model, for both triggering times. The calculated energy conversion ratios are typically one order of magnitude larger than those in steam explosion experiments with corium, where the energy conversion ratio may be only roughly estimated as it is not directly measured [2,6,7]. This could be an indication that the energy conversion ratio at the reactor scale may be larger than that at the experimental scale; a reason could be better explosion region confinement in reactor conditions due to the large scale.

6. Conclusion

A PWR and BWR ex-vessel steam explosion analysis was performed with the MC3D code. In this study, conditions of the OECD SERENA project reactor exercise were considered for the PWR and BWR central melt release cases. The main differences between both cases are that the reactor cavity, melt free fall height, and water depth in the BWR case are significantly more than those in the PWR case. In reactor calculations, the largest uncertainties in the prediction of steam explosion strength are expected to be caused by the large uncertainties related to the jet breakup. These uncertainties propagate through different premixing processes, and result in uncertainties in the generation rate and size of the melt droplets, distribution of the melt droplets in the premixture, droplet solidification, and void fraction, which all influence the steam explosion strength. To get some insight into these uncertainties related to the jet breakup, the premixing simulations were performed with both available jet breakup models—the global model and the local KH model.

The performed simulations revealed that weaker explosions are predicted by the KH model, compared to the global model, due to the predicted smaller melt droplet size, resulting in increased melt solidification and increased void buildup, both reducing the explosion strength. In the PWR case, the explosion was triggered at the melt–bottom contact, whereas in the BWR case, two triggering times were considered: when the melt penetrated 3.6 m into the water, like in the PWR case, and at the time of the calculated maximum active melt mass, when the strongest steam explosion is expected. It was found that due to a faster melt penetration and shorter melt penetration time till explosion triggering, resulting in less melt solidification and less void buildup, the active melt mass at explosion triggering is significantly larger for the BWR case. However, despite the lower active melt mass for the PWR case, the pressure loads at the cavity walls are typically higher than those for the BWR case, even when the explosion was triggered at the time of the maximum active melt mass in the BWR case. The reason is the significantly larger BWR cavity, where the explosion pressure wave originating from the premixture in the center of the cavity has already been weakened significantly on reaching the distant cavity wall. For the PWR case, the predicted maximum pressure on the cavity wall is ~15 MPa with both jet breakup models. The maximum pressure impulse at the wall is ~110 kPa·second with the global model and ~80 kPa·second with the KH model. For the BWR case, the predicted maximum pressure at the wall is ~15–20 MPa with the global model and ~5–10 MPa with the KH model. For the most challenging BWR

case considered, the maximum pressure impulse at the wall is ~90 kPa·second with the global model and ~35 kPa·second with the KH model.

An important measure of the strength of a steam explosion is the mechanical work performed by it. The simulations showed that at similar active melt masses, the maximum kinetic energy is significantly larger for the PWR case than for the BWR case. The reason is that in the PWR case, the water level rises up to the reactor vessel, making venting of the explosion region more difficult and thus, due to longer confinement times, heat transfer from the active melt to the water is more completed than in the BWR case where the water surface is free. The energy conversion ratios based on the mass of corium in water are in the range of 1–3%, the largest being for the BWR case, applying the global jet breakup model, where a premixture enabling the development of the most efficient explosion forms due to a fast melt penetration in combination with large melt droplets. The calculated energy conversion ratios are typically one order of magnitude larger than those in steam explosion experiments with corium, which could be an indication that the energy conversion ratio is possibly larger at the reactor scale than at the experimental scale.

It is difficult to judge which of the applied jet breakup models produces more reliable results in reactor conditions. Both models were successfully validated by experimental results. The KH model is more mechanistic and thus potentially better suited for extrapolation from experimental conditions to reactor conditions; however, its limitation is that due to strong coupling of various nonlinear phenomena, an extrapolation far from the experimental conditions might not be very reliable. On the contrary, the robust global model is more parametric, thus enabling a more controlled behavior, but its drawback is that the eventual required extrapolation of the model parameters to the reactor scale has to be done by engineering judgment, which might not be very reliable either. For safety studies, it is thus important that we are aware of the FCI modeling uncertainties, which have to be dealt with by performing parametric analyses within a reasonable range of model parameters and by applying different validated modeling approaches if available. To be able to reduce the FCI modeling uncertainties and improve the reliability of reactor calculations, further experimental and analytical FCI research is required.

Conflicts of interest

All authors have no conflicts of interest to declare.

Acknowledgments

The authors acknowledge the financial support of the Slovenian Research Agency within the research program P2-0026.

REFERENCES

[1] M.L. Corradini, B.J. Kim, M.D. Oh, Vapor explosions in light water reactors, a review of theory and modelling, Prog. Nucl. Energy 22 (1988) 1–117.
[2] G. Berthoud, Vapour explosions, Annu. Rev. Fluid Mech. 32 (2000) 573–611.
[3] T.G. Theofanous, The study of steam explosions in nuclear systems, Nucl. Eng. Des. 155 (1995) 1–26.
[4] H. Esmaili, M. Khatib-Rahbar, Analysis of likelihood of lower head failure and ex-vessel fuel coolant interaction energetics for AP1000, Nucl. Eng. Des. 235 (2005) 1583–1605.
[5] M. Leskovar, M. Uršič, Estimation of ex-vessel steam explosion pressure loads, Nucl. Eng. Des. 239 (2009) 2444–2458.
[6] M.L. Corradini, Vapor explosions: a review of experiments for accident analysis, Nucl. Saf. 32 (1991) 337–362.
[7] I. Huhtiniemi, D. Magallon, H. Hohmann, Results of Recent KROTOS FCI tests: aluminia versus corium melts, Nucl. Eng. Des. 189 (1999) 379–389.
[8] S.W. Hong, P. Piluso, M. Leskovar, Status of the OECD-SERENA Project for the resolution of ex-vessel steam explosion risks, J. Energy Power Eng. 7 (2013) 423–431.
[9] M. Leskovar, S. Basu, C. Brayer, M. Buck, M. Bürger, M. Corradini, R. Meignen, SERENA Analytical Working Group Outcome Document, OECD/NEA SERENA AWG/Sec/(14)1, 2014.
[10] R. Meignen, S. Picchi, J. Lamome, B. Raverdy, S.C. Escobar, G. Nicaise, The challenge of modeling fuel–coolant interaction: part I—premixing, Nucl. Eng. Des. 280 (2014) 511–527.
[11] R. Meignen, B. Raverdy, S. Picchi, J. Lamome, The challenge of modeling fuel–coolant interaction: part II—steam explosion, Nucl. Eng. Des. 280 (2014) 528–541.
[12] D. Magallon, I. Huhtiniemi, Corium melt quenching tests at low pressure and subcooled water in FARO, Nucl. Eng. Des. 204 (2001) 369–376.
[13] R. Meignen, Analysis of FARO Premixing Calculations with MC3D in View of Reactor Applications for the PSA Level 2 V2, IRSN Report, DPEA/SEAC/03-026, 2004.
[14] D. Magallon, SERENA Programme Reactor Exercise, Synthesis of Calculations, Report, 2012.
[15] J.M. Seiler, B. Tourniaire, F. Defoort, K. Froment, Consequences of material effects on in-vessel retention, Nucl. Eng. Des. 237 (2007) 1752–1758.
[16] GEMINI2: Gibbs Energy MINImizer User Guide, THERMODATA-INPG-CNRS, France, 2003.
[17] NUCLEA-09, Thermodynamic Database, THERMODATA, 2009.